JOURNAL OF SPACECRAFT AND ROCKETS
Vol. 37, No. 4, July–August 2000

Continuum and Kinetic Simulation of Laminar Separated Flow at Hypersonic Speeds

G. N. Markelov,* A. N. Kudryavtsev,† and M. S. Ivanov‡
Russian Academy of Sciences, 630090, Novosibirsk, Russia

The continuum and kinetic approaches were used to study the shock wave/boundary-layer interaction for monoatomic and diatomic gases. The effect of the translational/rotational exchange and gas/surface interaction models for the kinetic approach on the flow structure was analyzed. The influence of slip conditions for the Navier–Stokes solver on the shock wave position and separation region length was studied. A comparison with available experimental data was performed.

Nomenclature

C_f = skin friction coefficient
C_p = pressure coefficient
Kn = Knudsen number, λ/L
L = reference length, m
M = Mach number
N_c = number of collisional cells
N_p = total number of model particles
n = normal to the solid wall
Pr = Prandtl number
p = pressure, Pa
Re = Reynolds number
St = Stanton number
T = temperature, K
U = flow velocity, m/s
U_τ = velocity component tangential to the solid wall
X = distance from the leading edge in the freestream direction
X_{reat} = location of reattachment point
X_{sep} = location of separation point
Y = distance from the wall
Z_R = rotational collision number
α_e = energy accomodation coefficient
α_u = tangential moment accommodation coefficient
γ = specific heat ratio
ΔX = separation region length
λ = mean free path, m
μ = coefficient of viscosity
ρ = density, kg/m^3
ω = exponent in power-law dependence of the viscosity on the temperature

Subscripts

g = gas quantity at the wall
s = slip
w = wall
0 = stagnation quantity
∞ = freestream quantity

Presented as Paper 99-3527 at the AIAA 38th Fluid Dynamics Conference, Norfolk, VA, 28 June–1 July 1999; received 5 October 1999; revision received 16 February 2000; accepted for publication 6 March 2000.

*Senior Research Scientist, Computational Aerodynamics Laboratory, Institute of Theoretical and Applied Mechanics, Siberian Division; markelov@itam.nsc.ru.

†Senior Research Scientist, Computational Aerodynamics Laboratory, Institute of Theoretical and Applied Mechanics, Siberian Division.

‡Head, Computational Aerodynamics Laboratory, Institute of Theoretical and Applied Mechanics, Siberian Division. Senior Member AIAA.

Introduction

ONE of the most challenging problems of hypersonic aerodynamics is the shock wave/boundary-layerinteraction. This interaction can cause the formation of a separation region and can lead, for example, to a decrease in the control surface efficiency and to an increase in the heat flux on the wall in the vicinity of the reattachment point.

Numerical analysis of this problem is traditionally performed using Navier–Stokes (NS) equations. For low-to-moderate Reynolds numbers, slip conditions should be used to take into account the initial effects of rarefaction. However, even with slip conditions, the NS equations are inapplicable in the vicinity of the leading edge of slender bodies, especially for small angles of attack (see Ref. 1 for details).

The shock wave/laminar boundary-layer interaction under ONERA R5Ch wind-tunnel conditions ($Re = 1.8916 \times 10^4$) was experimentally studied.[2,3] An axisymmetric hollow-cylinder flare configuration (Fig. 1) was used. In Refs. 2 and 3, the pressure and heat fluxes on the model surface were measured, the separation region length was determined using oil-flow visualization, and the density profiles in several cross sections were obtained by electron beam fluorescence. Because of these detailed studies, a hollow-cylinder flare was chosen for verification of numerical methods at the First Europe–U.S. High Speed Flow Field Database Workshop (Part II), 1997; and the First Eastern–Western High Speed Flow Field Conference and Workshop, 1998.

The following numerical solutions were presented at the 1997 workshop: 10 solutions obtained by NS solvers and two solutions obtained by direct simulation Monte Carlo (DSMC) methods. All reported NS computations were made with no-slip boundary conditions and gave a greater length of the separation region compared with DSMC and experimental results.[4] The DSMC results presented show that rarefaction effects are observed even for $Re \sim 2 \times 10^4$ with strong nonequilibrium of the flow near the leading edge and the body surface, as well as a significant velocity of the gas near the cylinder surface (at least 10% of the freestream velocity). Therefore, to reduce the difference between the NS results and experimental data, it is necessary to take into account the flow rarefaction using the slip boundary conditions. This was done in Ref. 5, and the preliminary results demonstrated a noticeable effect of slip conditions on the separation region length.

The main objectives of the present work are to study an axisymmetric shock wave/laminar boundary-layer interaction for a low Reynolds number flow by kinetic and continuum approaches, to analyze the influence of translational/rotational exchange and gas/surface interaction models for the DSMC method on the flow structure and to examine the applicability of slip conditions for NS equations for hypersonic flows of diatomic and monoatomic gases.

Flow Conditions

The computations were carried out for the ONERA R5Ch wind-tunnel conditions. For the stagnation conditions $p_0 = 2.5 \times 10^5$ Pa

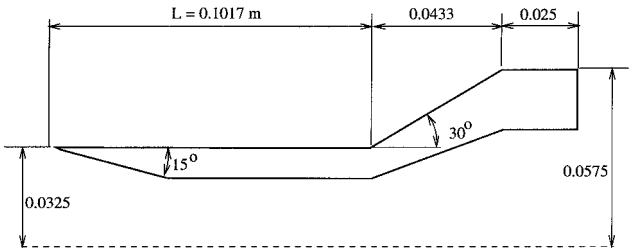

Fig. 1 Hollow-cylinder flare configuration.

and $T_0 = 1050$ K, the freestream Mach number $M_\infty = 9.91$, static temperature $T_\infty = 51$ K, and static pressure $p_\infty = 6.3$ Pa. The model surface is assumed to have a constant surface temperature of $T_w = 293$ K.

Figure 1 shows a hollow-cylinder flare. The hollow cylinder has a sharp leading edge with bevel angle of 15 deg and is aligned parallel to the oncoming flow. The compression flare is inclined at 30 deg to the cylinder and is terminated by a hollow cylindrical section. The total length of the model is 0.17 m. The reference length $L = 0.1017$ m is the distance from the leading edge to the flare.

The Reynolds number calculated with L is $Re = 1.8916 \times 10^4$. Nitrogen was used as a test gas, and the mean free path $\lambda_\infty = 9.5103 \times 10^{-4}$ m is defined from freestream conditions.[6] The Knudsen number $Kn = \lambda_\infty / L = 9.35 \times 10^{-4}$.

To evaluate the adequacy of slip conditions for high-speed flows, additional calculations were conducted for a monoatomic gas (argon) and Mach numbers $M_\infty = 2$ and 10. Static pressure and temperature are equal to the corresponding values of the R5Ch conditions.

Numerical Approaches

Kinetic Approach

The direct simulation Monte Carlo (DSMC) method[7] is used in the present paper. It is a method of computer simulation of the behavior of a great number of model particles (hundreds of thousands and millions). The DSMC computations were performed using an axisymmetric variant of the SMILE code[8] developed at the Institute of Theoretical and Applied Mechanics and based on cell and free-cell majorant frequency schemes.[9]

A number of numerical techniques to speed up calculations at low Knudsen numbers are used in SMILE (see Ref. 8 for details). For example, this code employs two independent grids adapted in the course of computation: the first one to organize particle collisions and the second one for sampling of macroparameters. Both grids are based on uniform rectangular background cells, which are split into smaller cells, if necessary. The use of background cells as a cluster of a certain number of collisional cells is convenient for many purposes. For example, to increase the efficiency of the particle movement procedure, the background cells containing the body surface and their neighbors are marked by a special flag. Thus, the particles cannot traverse this layer of cells surrounding the body during one time step, and the particle/surface collisions are checked only for marked cells. It is also convenient (and sometimes necessary, for example, for jet exhaust) in each background cell to use its own time step, particle weight, etc.

To reduce the computational time needed for the flow to become steady, a particle doubling procedure was used, which implies a sequential doubling of particles at earlier defined time steps.

The following models were used in the calculations: variable hard sphere[7] (VHS) model for intermolecular collisions, Larsen–Borgnakke model[10] for the energy exchange between translational and internal molecular modes with constant and temperature-dependent rotational collision number Z_R (for example, see Ref. 7), and diffuse gas/surface interaction model with complete and incomplete accommodation of energy.

To simulate the incomplete accommodation of translational energy, the coefficient of energy accommodation was used[1]:

$$\alpha_e = (E_i - E_r)/(E_i - E_w) \tag{1}$$

where E_i is the energy brought by incident molecules, E_r is the energy carried away by reflected molecules, and E_w is the energy that would be carried away by reflected molecules if the gas were in equilibrium with the wall. In each particle/surface collision, the Maxwellian distribution parameters are determined. The reflected particle velocities are sampled in accordance with this distribution.

In studying the applicability of slip conditions for NS equations, it is important to compare the slip velocity with the real-gas velocity near the body surface. To obtain the gas parameters F in the immediate vicinity of the wall, the following sampling procedure based on particle intersections with the body surface was used:

$$F = \left[\sum_{i=1}^{N} F^i \frac{1}{U_n^i}\right] \Bigg/ \left[\sum_{i=1}^{N} \frac{1}{U_n^i}\right] \tag{2}$$

where N is the number of intersection events and U_n^i is particle component of velocity normal to the surface.

Continuum Approach

The continuum calculations were performed using an axisymmetric version of the NS code developed at the Computational Aerodynamics Laboratory of the Institute of Theoretical and Applied Mechanics. The code solves the full laminar compressible NS equations with both no-slip and slip boundary conditions. It uses a structured grid with quadrilateral cells, which was stretched in the normal direction, so that grid nodes were concentrated in the boundary layer near the solid wall.

The code is based on the finite volume total variation diminishing scheme for the convective terms and the second-order central difference approximation of the diffusive terms. The inviscid fluxes are computed by the Harten–Lax–van Leer–Einfeld modified (HLLEM) Riemann solver.[11] The HLLEM solver preserves the robustness of the original HLLE solver[12] for simulation of high-speed flows, and at the same time, it does not suffer from the excessive numerical diffusion inherent in the HLLE method. As a result, the HLLEM solver is very appropriate for numerical simulation of viscous hypersonic flows.

High-order accuracy is obtained by applying the standard van Leer's formula of second/third order and the minmod slope limiter[13] for the reconstruction of the cell-face values of the primitive variables ρ and p and the velocity components from the cell-averaged ones.

Time marching is performed by employing the explicit Runge–Kutta scheme of second order. No techniques for acceleration of the convergence were used because it is possible that unsteady phenomena may play an important role in this problem, which includes the flow separation, and therefore, time-accurate simulation seems to be a more correct approach.

The computations were conducted using the perfect-gas model. The power-law dependence of the viscosity on the temperature $\mu \propto T^\omega$ was taken for a more straightforward comparison with the results of DSMC simulations. For the monoatomic gas (argon) ω was fixed as 0.81 and Prandtl number Pr was equal to 2/3. For calculations with nitrogen, $\omega = 0.75$ and $Pr = 0.72$. Note that using the Sutherland or power law dependences of the viscosity on the temperature gives practically the same results.

There is a great number of slip boundary conditions in the literature, which, as a rule, differ only slightly one from another. In the present paper, the slip velocity and temperature jump conditions deduced by Kogan[1] were employed. They can be written as

$$U_s = \frac{2 - a_u \alpha_u}{\alpha_u} \lambda \left(\frac{\partial U_\tau}{\partial n}\right)_s \tag{3}$$

$$T_s - T_w = \frac{2 - a_e \alpha_e}{2\alpha_e} \frac{\gamma}{\gamma - 1} \frac{1}{Pr} \lambda \left(\frac{\partial T}{\partial n}\right)_s \tag{4}$$

$$\lambda = \sqrt{(\pi/2)}\left(\mu \Big/ \sqrt{p\rho}\right) \tag{5}$$

Because no reliable data are available for α_u and α_e values at the present experimental conditions, both coefficients were taken equal

to unity. Furthermore, the numerical coefficients $a_u = 0.858$ and $a_e = 0.827$ are deduced from the approximate solution of the Boltzmann equation in the Knudsen layer near the solid wall.[1]

When numerically imposing these boundary conditions, the value of the local mean free path on the wall was evaluated by a linear extrapolation from within the domain, and Eqs. (3–5) were solved to calculate U_s and T_s. After that, the computed values were used to calculate (by means of a linear extrapolation) quantities in ghost cells outside the computational domain.

Results and Discussion

DSMC Computations

A vast separation region is formed in the flow around a hollow-cylinder flare under R5Ch wind-tunnel conditions. This region is clearly seen in Fig. 2, which shows the streamlines. A separation shock wave starts to form over the separation region and intersects the leading-edge shock wave over a point where the flare transforms into the cylindrical section (Fig. 3).

The effect of the numerical method parameters (the number of collisional cells and the total number of model particles) on the flow structure was studied. The separation region length was found to depend strongly on these parameters unless the number of collisional cells exceeds $N_c = 6 \times 10^5$ (Table 1).

The influence of the numerical method parameters was studied in detail[14,15]; only one example illustrating this influence is presented here. Figure 4 shows the density profiles for coarse ($N_c = 0.15 \times 10^6$, $N_p = 0.245 \times 10^6$) and fine ($N_c = 10^6$, $N_p = 4 \times 10^6$) grid cases in the cross section $X/L = 0.9$ ahead of the junction of the cylinder and the flare; the ordinate axis shows the distance from the body surface. An increase in the grid resolution leads to a decrease in the angle of inclination of the leading-edge shock wave. The formation of a separation shock wave for the fine-grid case begins at smaller X/L than for the coarse-grid case because of the different separation region length. This is the reason that the second peak of the density profile corresponding to the separation shock wave is observed in the cross section $X/L = 0.9$ only for the fine-grid case.

Table 1 Influence of grid and the number of particles for DSMC method on separation zone length ($X_{sept}/L - X_{reat}/L$, $Z_R = 5$)

Number of collisional cells N_c	Total number of model particles N_p				
	245,000	490,000	980,000	1,950,000	4,000,000
150,000	0.87–1.25	0.84–1.28	——	——	——
370,000	——	0.82–1.28	0.81–1.29	——	——
600,000	——	——	——	0.80–1.30	——
1,000,000	——	——	——	——	0.79–1.30

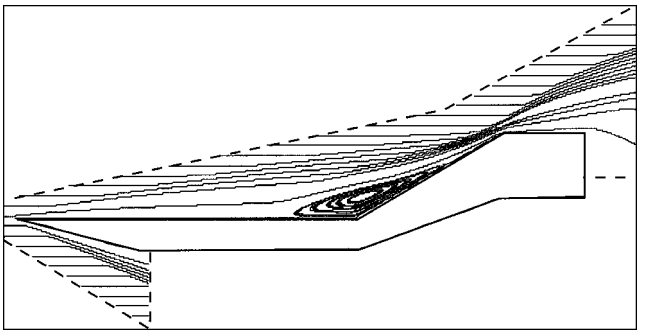

Fig. 2 Selected streamlines: DSMC method, $Z_R = 5$, and $\alpha_e = 1.0$.

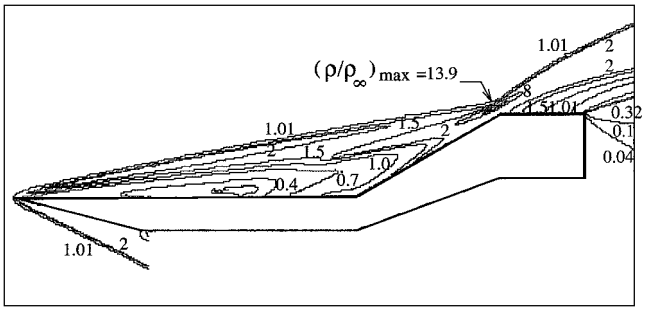

Fig. 3 Density contours: DSMC method, $Z_R = 5$, and $\alpha_e = 1.0$.

Table 2 Influence of models for DSMC method on separation zone length

Z_R	α_e	X_{sep}/L	X_{reat}/L
5	1.0	0.79	1.30
5	0.5	0.78	1.34
Temperature dependent	1.0	0.77	1.32

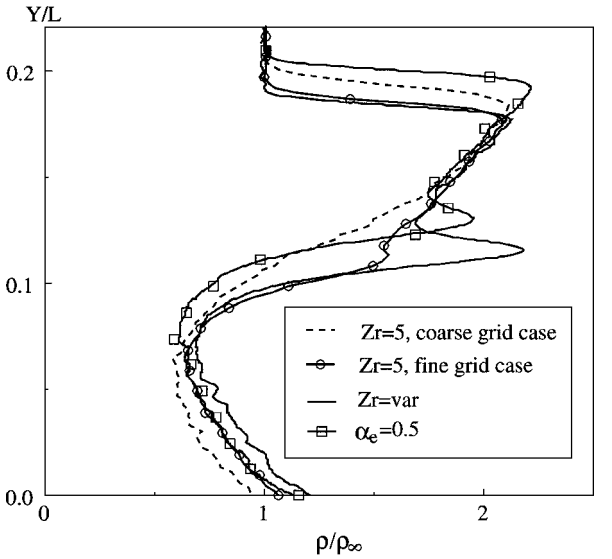

Fig. 4 Influence of grid and models for DSMC method on density profiles at $X/L = 0.9$.

The DSMC results presented subsequently were obtained using $N_c \sim 10^6$ collisional cells. The radial size of the cells was smaller by a factor of 5–10 than that along the X axis to catch weak flow gradients near the cylindrical portion of the model.

Energy Accommodation Effect

Incomplete energy accommodation exerts a significant effect at high Knudsen numbers when a gas molecule experiences no more than one collision with the body surface. As the Knudsen number decreases, the molecule can experience several collisions. Each collision decreases the difference between the energy of a reflected particle and the energy of a particle reflected in equilibrium with the wall. As a result, the effective value of the energy accommodation coefficient is smaller than α_e and depends on the number of particle collisions, m, with the surface[16]:

$$\tilde{\alpha}_e = 1 - (1 - \alpha_e)^m \tag{6}$$

For $Kn \sim 10^{-3}$ being considered, one can anticipate that the effect of α_e on the overall flow field is negligibly small and noticeable only in the vicinity of the leading edge.

The calculations for $\alpha_e = 0.5$ show that the energy accommodation coefficient exerts a significant effect on the overall flowfield. The decrease in α_e from 1 to 0.5 had practically no effect on the flow separation point, but enlarged the separation region length due to the downstream shift of the reattachment point (Table 2). The slope of the leading-edge shock wave increased (Fig. 4), which caused a 20% increase in the pressure coefficient C_p (Fig. 5). Incomplete energy accommodation led to a decrease in the heat flux (Fig. 6), which is related to an increase in the energy of reflected particles. A similar effect can be obtained by increasing the body temperature T_w. Thus, accounting for incomplete energy accommodation allows one to estimate a possible effect of the varied temperature of the

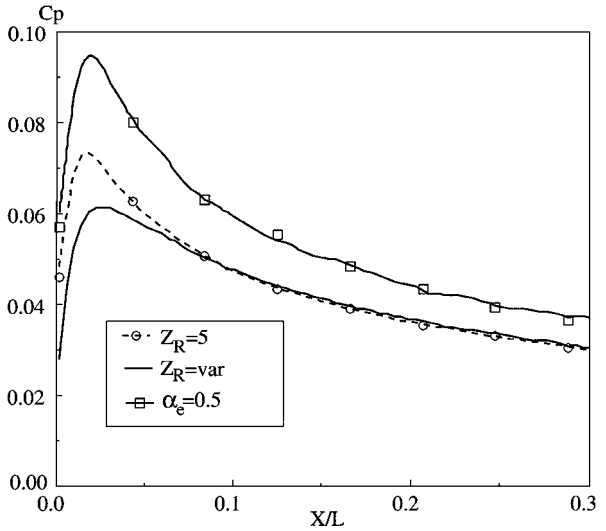

Fig. 5 Pressure coefficient in the vicinity of leading edge.

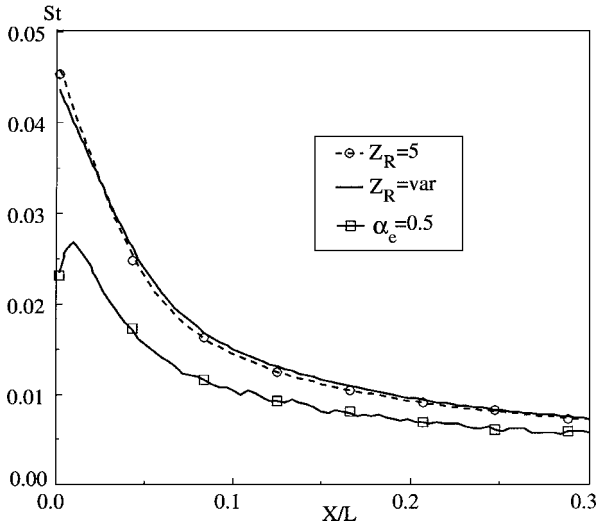

Fig. 6 Stanton number in the vicinity of leading edge.

body surface along X (high values of T_w near the leading edge) under experimental conditions.

Effect of Translational/Rotation Exchange

The earlier calculations were conducted for constant values of rotational and vibrational collision numbers $Z_R = 5$ and $Z_V = 50$, respectively. It is known that Z_R and Z_V depend on the flow temperature.[7] Calculations with temperature-dependent Z_R were conducted, that is, the temperature in each cell was determined, and the corresponding value of Z_R was used for energy exchange between translational and rotational molecular modes. The influence of Z_V was not considered because the excitation of vibrational degrees of freedom of molecules is practically unobserved for the temperature range examined (less than 1050 K).

The calculations show that $Z_R \sim 2$ in the major part of the computational domain; only near the body surface and in the region of interaction of the leading edge and separation shock waves does the rotational collision number reach the value $Z_R \sim 4$. The most pronounced effect of the temperature-dependent Z_R was observed for the value of C_p in the vicinity of the leading edge (see Fig. 5), whereas the heat flux magnitude remained the same (see Fig. 6). The leading-edge shock wave position also remained almost unchanged, but the separation shock wave strength increased significantly. For example, the density behind the separation shock wave in the cross section $X/L = 0.9$ (Fig. 4) is greater by 8% than the density behind the leading-edge shock wave. The separation region length also became somewhat greater as compared with the $Z_R = 5$ case

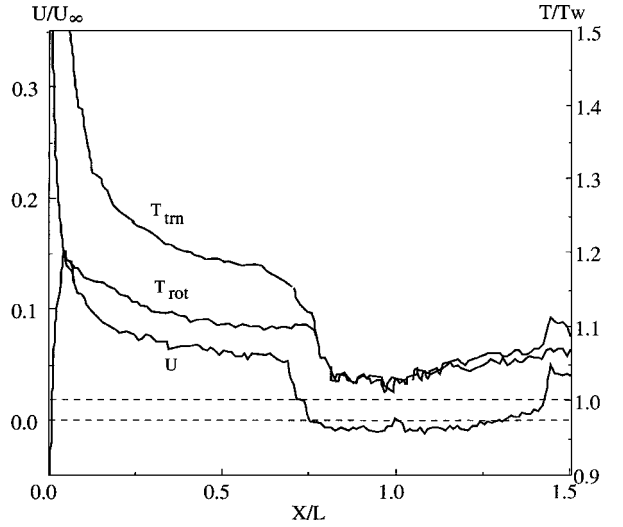

Fig. 7 Gas velocity U and translational T_{trn} and rotational T_{rot} temperatures at the wall.

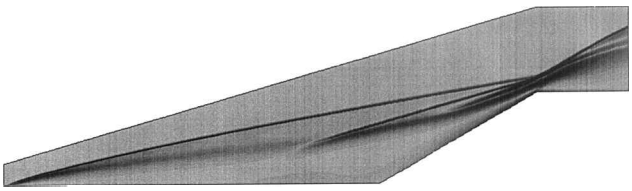

Fig. 8 Numerical schlieren picture: NS solver.

(see Table 2). In the subsequent comparison with NS results and experimental data, the DSMC results obtained for the temperature-dependent Z_R were used.

Gas Parameters Near the Wall

The use of a sampling procedure based on particle intersections with the body surface allowed us to obtain the flow parameters immediately near the body surface. Figure 7 shows the gas velocity and the translational and rotational temperatures of the gas near the surface. It is seen that the gas velocity is significantly different from zero near the cylinder surface. The gas velocity decreases with distance from the leading edge and equals approximately 8% of the oncoming flow velocity ($U_\infty = 1443$ m/s) upstream of the separation region. Inside the separation region, this velocity is small and negative. In the subsequent expansion of the flow behind the flare, the gas velocity increases again to 5% of U_∞.

The gas temperature is also noticeably different from the wall temperature T_w. In this case, the translational and rotational temperatures have different values, and the difference reaches a factor of four in the vicinity of the leading edge. The temperature values almost coincide inside the separation region and are close to T_w. Rarefaction effects are significant even for moderate Reynolds number $Re \sim 2 \times 10^4$ in the flow around a hollow cylinder at zero incidence.

NS Computations

The numerical schlieren picture for the hollow-cylinder flare configuration is presented in Fig. 8. It clearly shows shock waves, the line dividing the inviscid flow behind the leading-edge shock wave and the boundary layer, and the line dividing the inviscid flow behind the separated shock wave and the separation bubble. The shock wave arising due to flow reattachment is almost parallel to the flare surface and is distinctly shown in Fig. 9.

An accurate simulation of high-speed separated flows is still a difficult problem for modern numerical techniques. In particular, the investigations performed by participants of high-speed flow database workshops,[17] computed by different codes, showed substantial differences in the separation point position, and, as a consequence, in many other important characteristics.

For this reason, we started our investigation with an analysis of the influence of grid resolution. The results of computations conducted

Table 3 Separation region length for NS calculations with no-slip boundary conditions on different grids

Grid	X_{sep}/L	X_{reat}/L
160 × 67	0.802	1.266
240 × 100	0.748	1.314
360 × 150	0.735	1.327
480 × 200	0.703	1.348
DSMC	0.77	1.32
Experiment	0.76 ± 0.01	1.34 ± 0.015

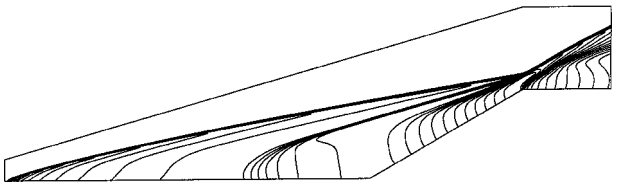

Fig. 9 Pressure contours: NS solver.

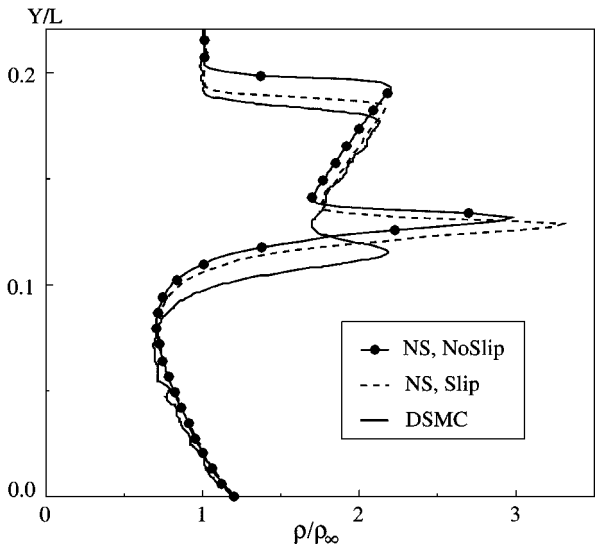

Fig. 10 Density profiles at $X/L = 0.9$.

on different grids using no-slip boundary conditions are given in Table 3.

It is evident that the separation zone length increases when the grid is refined. This tendency was also noticed when results of high-speed flow database workshops were analyzed. We believe that the values obtained in the present paper on the most refined grid can be considered as close to asymptotic, grid-independent values. It can be confirmed by the comparison with the most resolved computations from Ref. 17, as well as by very close agreement between our results and those of the very careful investigation by Walpot (L. Walpot, private communication, 1998). However, note that the results disagree with the data from the DSMC simulations and experimental investigations. The substantial difference can be observed not only for locations of the separation and reattachment points, but also for the distance between the leading-edge shock and the body surface. Figure 10 shows the density distributions in the cross section $X/L = 0.9$. It is seen that the leading-edge shock calculated by the NS code with no-slip is situated noticeably higher than in the DSMC simulation.

One possible reason for this disagreement may be the influence of rarefaction effects, in particular, the slip velocity and the temperature jump on the body surface. Indeed, the Knudsen number based on the boundary-layer thickness δ, which is a natural length scale for this problem, can be estimated as

$$Kn_\delta \approx M/Re_\delta \sim M\sqrt{Re} \approx 7 \times 10^{-2} \tag{7}$$

For this value the rarefaction effects should be quite significant. Therefore, the computations were repeated on the most refined grid using the slip boundary conditions (3) and (4). It can be seen from Fig. 10 that the position of the leading-edge shock wave resulting from the NS calculations with the slip boundary conditions is substantially closer to the DSMC value than with no-slip. In fact, this position almost coincides with that obtained in the DSMC simulations with $Z_R = 5$ (not shown), but the computation using the temperature-dependent Z_R gives the shock wave even closer to the body. Satisfactory agreement with the DSMC results is also achieved for the distributed characteristics on the body surface. Figure 11 shows the distributions of the pressure and friction coefficients and the Stanton number, whose definition

$$St = \frac{[\mu U_\tau(\partial U_\tau/\partial n) + k(\partial T/\partial n)]_s}{\rho_\infty U_\infty (H_0 - H_w)} \tag{8}$$

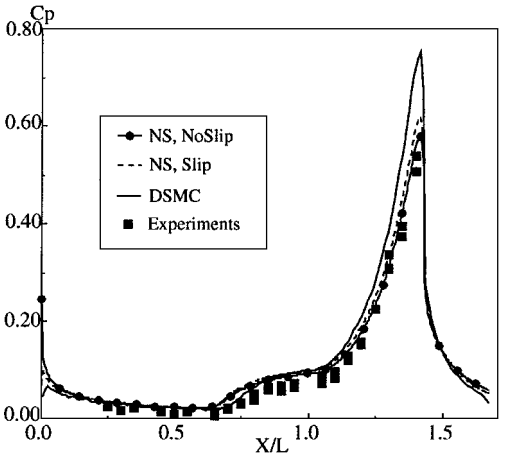

a) Pressure coefficient

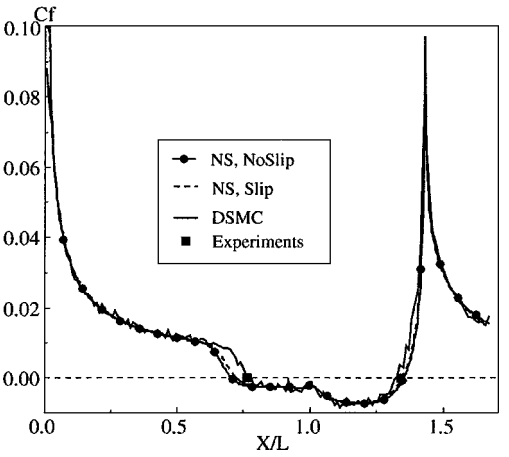

b) Skin-friction coefficient

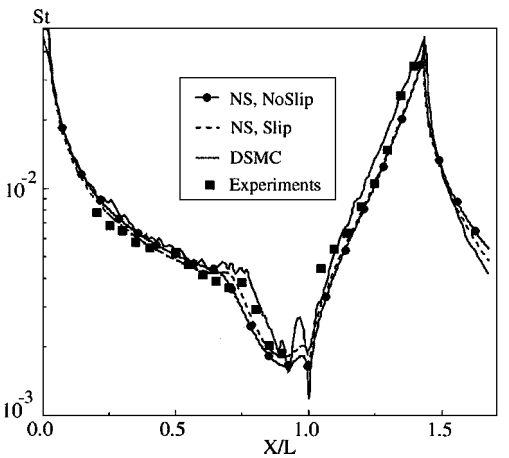

c) Stanton number

Fig. 11 Distributed parameters.

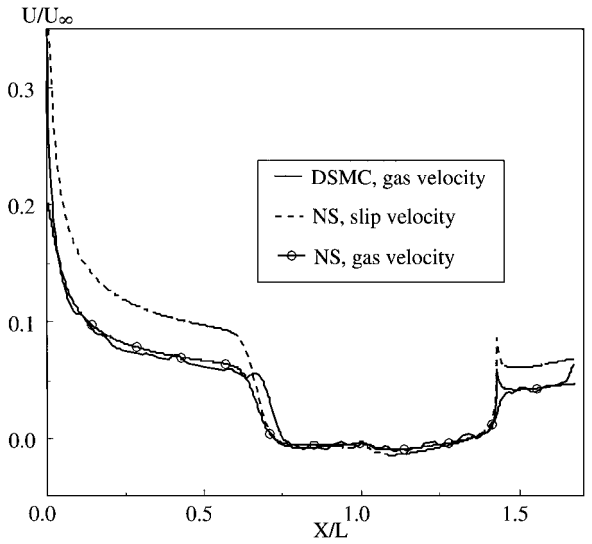

Fig. 12 Slip and gas velocity at the wall.

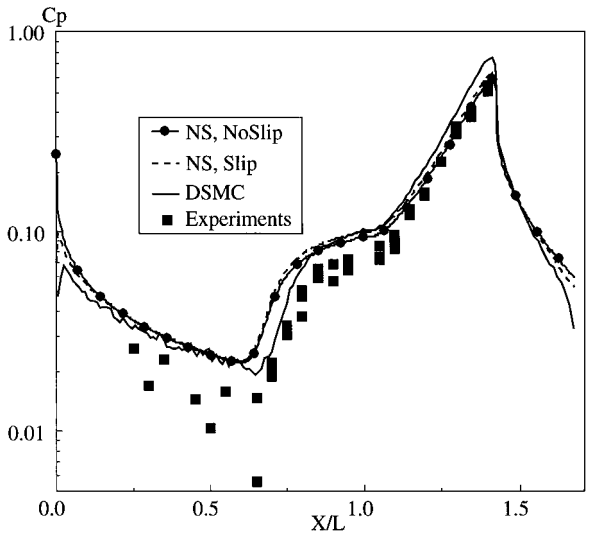

Fig. 13 Pressure coefficient distribution.

takes into account nonvanishing gas velocity on the wall. Here k is the heat conductivity, and H is the enthalpy.

Nevertheless, the location of the separation point, as before, differs significantly from the DSMC and experimental values. Namely, the NS computations with slip boundary conditions give $X_{sep}/L = 0.723$. The possible reasons may include the rotational/translational nonequilibrium, which is neglected when deriving the NS equations or the inadequacy of slip boundary conditions (3) and (4) at hypersonic Mach numbers. We consider this subject in more detail.

Slip Velocity

In Fig. 12, the slip velocity distribution along the surface for both the DSMC and the NS computations is given. Note that the NS slip velocity U_s does not agree with the gas velocity on the wall resulting from the DSMC simulations. This disagreement is predicted by the kinetic theory. In fact, the slip velocity is defined by Eq. (3) in such a way that the continuum and kinetic solutions should coincide outside the Knudsen layer. Inside the Knudsen layer, however, they should differ. In accordance with Ref. 18, the velocity distribution across the Knudsen layer can be written as follows:

$$U_\tau(Y) = A\left[Y + \eta - \lambda\mathcal{I}\left(\sqrt{\pi}Y \mid 2\lambda\right)\right] \tag{9}$$

where $\eta \approx 1.1466\lambda$. The first two terms in the brackets give the NS solution, and the third term is a kinetic correction. The function $\mathcal{I}$ is an integral, which cannot be reduced to the elementary functions. Its value at $Y = 0$, however, can be calculated exactly, which gives the following formula for the real gas velocity on the wall U_g:

$$U_g = \sqrt{(2/\pi)}A\lambda \tag{10}$$

As a result, we obtain the simple relation between U_g and $U_s = A\eta$:

$$U_g = \sqrt{(2/\pi)}(1/1.1466)U_s = 0.696U_s \tag{11}$$

The gas velocity U_g calculated from U_s with the help of this formula is shown in Fig. 12. It is in excellent agreement with the DSMC result.

Comparison of Numerical Results with Experimental Data

A comprehensive experimental study of flow near a hollow-cylinder flare was performed.[2] The pressure and heat flux distributions on the model surface were measured, the separation region length was determined, and the density profiles were plotted in several cross sections.[3]

A detailed comparison with the experimental data for the distributed aerothermodynamic characteristics, C_p, C_f, and Stanton number, is shown in Fig. 11. The separation region length predicted by the DSMC method coincides with the experimental value within the experimental error. The NS equations with slip conditions predict a somewhat greater length of the separation region. Numerical results for the distribution of Stanton numbers St along the body obtained with the two approaches agree quite well with the corresponding measured values. At the same time, numerical simulation predicts the pressure value higher than the measured result both on the flare surface (see Fig. 11a) and on the hollow cylinder surface, which is clearly seen if a logarithmic scale is used (Walpot, private communication) (Fig. 13).

A comparison of numerical results with measured density profiles is shown in Fig. 14. In the cross section $X/L = 0.3$, the DSMC and NS with slip conditions are in good agreement with experimental data. For a greater distance from the leading edge, numerical simulation predicts a smaller inclination of the leading-edge shock wave than the experimentally measured value. The calculated density inside the boundary layer are slightly different from experimental data for $X/L = 0.6$, but are in excellent agreement for $X/L = 0.76$.

Note that the experimental shock wave position almost coincides with the solution of NS equations with no-slip conditions for $X/L = 0.6$ and 0.76. This behavior of the experimental data requires further investigation, with additional experimental studies.

Comparison of DSMC and NS Results for a Monoatomic Gas

The differences observed between DSMC and NS results for the R5Ch wind-tunnel conditions are also possibly caused by translational/rotational nonequilibrium of the flow. To evaluate the applicability of slip conditions for hypersonic flow, a series of computations was conducted for a monoatomic gas (argon).

The profiles of the flow parameters in several cross sections are shown in Fig. 15. As in the case of a diatomic gas, the use of slip conditions for the NS solver reduces the slope of the leading-edge shock wave and yields fair agreement with the DSMC results in terms of density and velocity profiles. However, the temperatures inside the boundary layer for DSMC and NS with slip conditions differ by 20%. This can be related to that the continuum approach is inapplicable in the vicinity of the leading edge, where strong nonequilibrium of the flow is observed, even taking into account slip conditions. The difference in the translational temperature along different directions can be used as a criterion of flow nonequilibrium. Figure 16 shows the deviation of the longitudinal temperature from its mean value. A 30% deviation of T_x/T is observed up to $X/L = 0.1$. The magnitude of T_x/T decreases downstream, but is still noticeable at a distance $X/L = 0.4$, which corresponds to $400\lambda_\infty$. Note that the distribution of T_x/T has a maximum inside the boundary layer, and the position of this maximum coincides with the iso-Mach line $M = 1$.

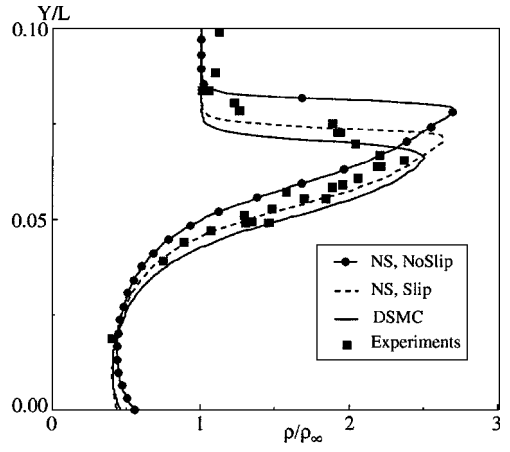

X/L = 0.3

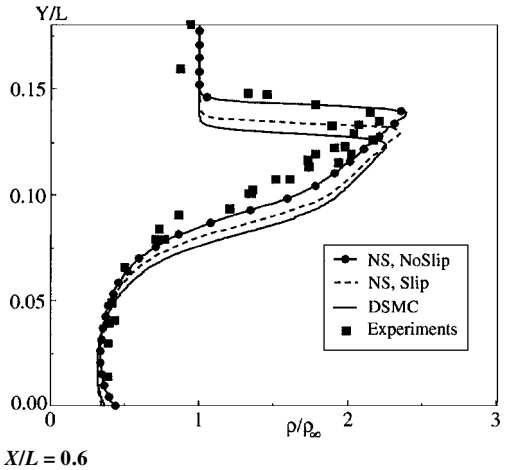

X/L = 0.6

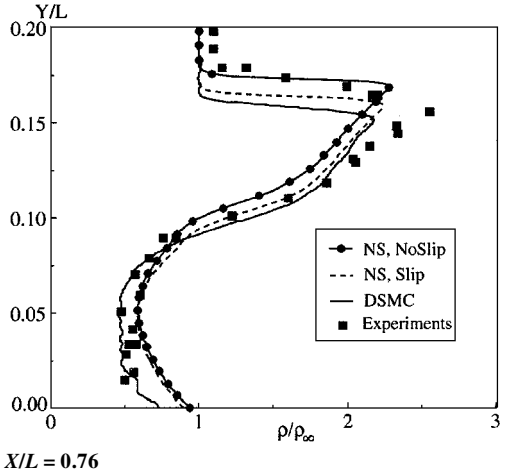

X/L = 0.76

Fig. 14 Density profiles.

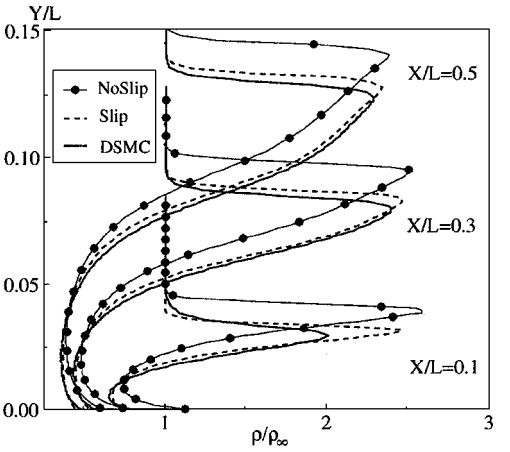

Density profiles

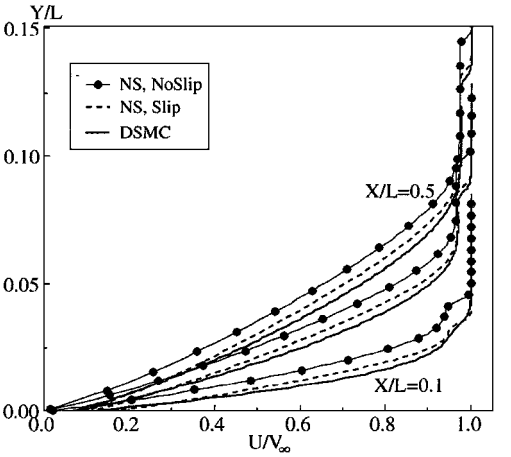

Velocity profiles

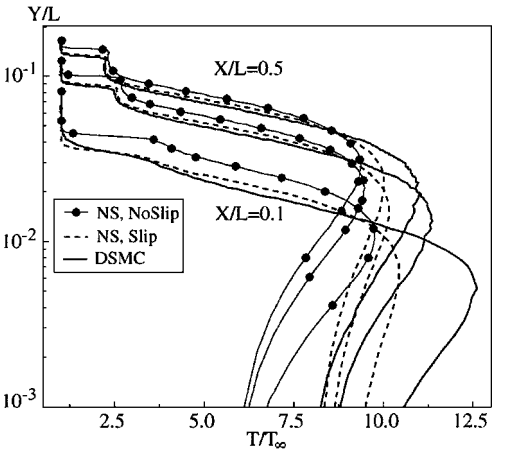

Temperature profiles

Fig. 15 Flow parameters at *X/L* = 0.1, 0.3, and 0.5; argon, M_∞ = 10.

Strong nonequilibrium of the flow in the vicinity of the leading edge is the reason that the NS solver with no-slip and slip conditions predicts a significantly greater heat flux (up to a factor of four) than the DSMC method (Fig. 17). This is responsible for the decrease in flow temperature downstream.

The mentioned differences also affect the separation region length. Its NS value is slightly larger ($\Delta X/L = 0.534$ for a 160×67 grid) than the DSMC results ($\Delta X/L = 0.490$) and increases as the grid is further refined ($\Delta X/L = 0.541$ for a 240×100 grid).

A significant decrease in flow nonequilibrium is observed as the Mach number of the oncoming flow decreases. Therefore, the flow around a hollow cylinder for $M_\infty = 2$ was calculated to estimate the contribution of the slip conditions. The temperature profiles in Fig. 18 show that the use of slip conditions significantly affects the flow structure and allows excellent agreement with the DSMC

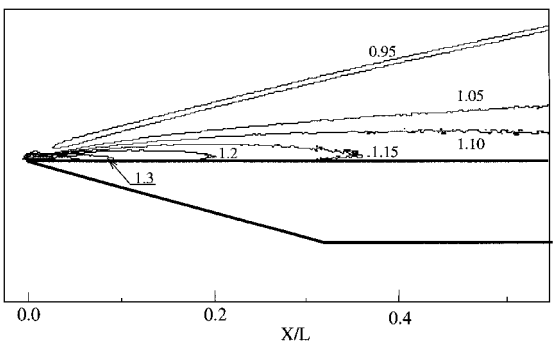

Fig. 16 Nonequilibrium of temperature, T_x/T: DSMC method.

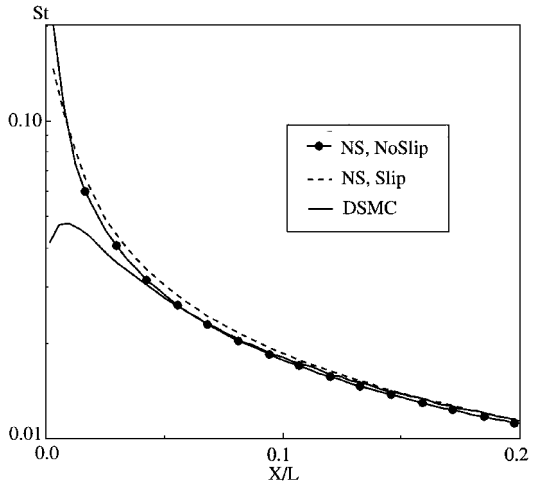

Fig. 17 Stanton number; argon, $M_\infty = 10$.

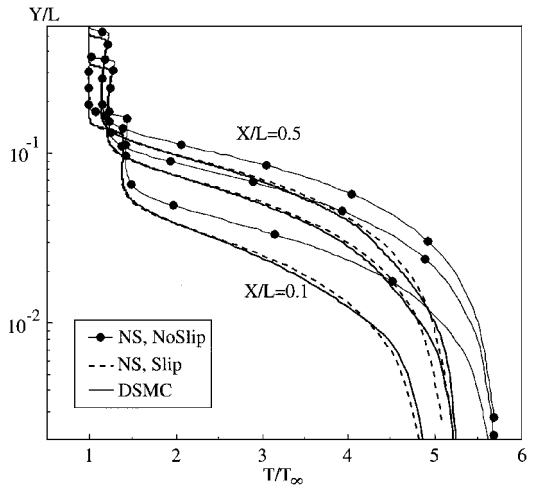

Fig. 18 Temperature profiles at $X/L = 0.1$, 0.3, and 0.5; argon, $M_\infty = 2$.

results. Hence, the inapplicability of NS equations for high Mach numbers in the vicinity of the leading edge affects the entire flowfield near a hollow-cylinder flare.

Conclusions

An axisymmetric shock wave/laminar boundary-layer interaction for the R5Ch wind-tunnel conditions was studied using the continuum (NS equations) and kinetic (DSMC method) approaches.

It is shown that incomplete accommodation of energy during particle collisions with the body surface leads to an increase in the leading-edge shock wave inclination and an insignificant increase in the separation region length.

The use of temperature-dependent rotational collision number has almost no effect on the leading-edge shock wave position, but significantly increases the separation shock wave strength, as well as somewhat increases the separation region length.

It is shown that the application of the classical conditions for slip velocity and temperature jump has a substantial effect on the entire flowfield and yields reasonable agreement with the DSMC results.

A comparison of numerical simulations with experimental data shows good agreement for the heat flux. However, the continuum and kinetic approaches overpredict the pressure values both on the flare and on the hollow-cylinder surface.

The density profiles measured for $X/L = 0.3$ are in good agreement with DSMC and NS with slip conditions, but for greater distances, the experimental data coincide with the NS equations with no-slip conditions. This behavior of the parameters requires further investigation, particularly experimental studies.

The conducted study of hypersonic flow around a hollow-cylinder flare for a monoatomic gas clearly showed that the NS equations, even with taking into account slip conditions, are inapplicable in the vicinity of the leading edge. The flow near the leading edge affects the flow structure downstream and, for example, leads to an increase in the separation region length.

Acknowledgments

This work was supported by Russian Foundation for Basic Research Grants 98-01-00677 and 98-01-00705 and by Lyapunov Center Project 2-97. This support is gratefully acknowledged.

References

[1]Kogan, N. M., *Rarefied Gas Dynamics*, Plenum, New York, 1969.

[2]Chanetz, B., "Study of Axisymmetric Shock Wave/Boundary Layer Interaction in Hypersonic Laminar Flow," ONERA, TR RT 42/4362 AN, 1995

[3]Gorchakova, N. G., Chanetz, B., Kuznetsov, L. I., Pigache, D., Pot, T., Taran, J. P., and Yarygin, V. N., "Electron-Beam-Excited X-ray Method for Density Measurements of Rarefied Gas Flows Near Models," *Proceedings of the XXI International Symposium on Rarefied Gas Dynamics*, CEPADUES-Editions, Marseille, France, 1999, pp. 591–598.

[4]Grasso, F., and Marini, M., "Synthesis of T2-97 Hollow Cylinder Flare Problem," *Proceedings of the First Europe–U.S. High Speed Flow Field Database Workshop, Part II*, AIAA, Reston, VA, 1998, pp. 213–221.

[5]Markelov, G. N., Kudryavtsev, A. N., and Ivanov, M. S., "Numerical Modeling of Near-Continuum Hypersonic Flow About a Hollow Cylinder Flare," *Proceedings of the XXI International Symposium on Rarefied Gas Dynamics*, CEPADUES-Editions, Marseille, France, 1999, pp. 647–654.

[6]Moss, J. N., Dogra, V. K, and Price, J. M., "DSMC Simulations of Viscous Interactions for Hollow Cylinder-Flare Configuration," AIAA Paper 94-2015, June 1994.

[7]Bird, G., *Molecular Gas Dynamics and the Direct Simulation of Gas Flows*, Clarendon, Oxford, 1994.

[8]Ivanov, M. S., Markelov, G. N., and Gimelshein, S. F., "Statistical Simulation of Reactive Rarefied Flows: Numerical Approach and Applications," AIAA Paper 98-2669, June 1998.

[9]Ivanov, M. S., and Rogasinsky, S. V., "Theoretical Analysis of Traditional and Modern Schemes of the DSMC Method," *Proceedings of the XVII International Symposium on Rarefied Gas Dynamics*, VCH, Aachen, Germany, 1991, pp. 629–642.

[10]Borgnakke, C., and Larsen, P. S., "Statistical Collision Model for Monte Carlo Simulation of Polyatomic Gas Mixture," *Journal of Computational Physics*, Vol. 18, No. 3, 1975, pp. 405–420.

[11]Einfeldt, B., Munz, C. D., Roe, P. L., and Sjögren, B., "On Godunov-Type Methods Near Low Densities," *Journal of Computational Physics*, Vol. 92, No. 2, 1991, pp. 273–295.

[12]Einfeldt, B., "On Godunov-Type Methods for Gas Dynamics," *SIAM Journal on Numerical Analysis*, Vol. 25, No. 2, 1998, pp. 294–318.

[13]Yee, H. C., "A Class of High-Resolution Explicit and Implicit Shock-Capturing Methods," NASA TM-101088, 1989.

[14]Markelov, G. N., and Ivanov, M. S., "Statistical Simulation of Laminar Hypersonic Flow About a Hollow Cylinder Flare," *Proceedings of the First Europe–U.S. High Speed Flow Field Database Workshop, Part II*, AIAA, Reston, VA, 1998, pp. 202–207.

[15]Moss, J. N., and Olejniczak, J., "Shock-Wave/Boundary-Layer Interactions in Hypersonic Low Density Flows," AIAA Paper 98-2668, June 1998.

[16]Roberts, J. K., "The Exchange of Energy Between Gas Atoms and Solid Surfaces," *Proceedings of the Royal Society of London, Series A: Mathematical and Physical Sciences*, Vol. 129, 1930, p. 146.

[17]Borrelli, S., Marini, M., Grasso, F., and Periaux, J. (eds.), *Proceedings of the First Europe–U.S. High Speed Flow Field Database Workshop, Part II*, AIAA, Reston, VA, 1998, Chap. T2-97.

[18]Cercignani, C., *Theory and Application of the Boltzmann Equation*, Scottish Academic, Edinburgh, 1975, Chap. 6.

R. G. Wilmoth
Associate Editor